

Delineation of the One Atmosphere Augite-Pigeonite Miscibility Gap for Pyroxenes from Lunar Basalt 12021¹

MALCOLM ROSS, J. S. HUEBNER, AND ERIC DOWTY²

U. S. Geological Survey, Washington, D. C. 20244

Abstract

Single crystals of lunar clinopyroxene containing a second exsolved clinopyroxene have been investigated by stepwise heating experiments combined with X-ray diffraction techniques. Results show that the pigeonite-augite two-phase region narrows with increasing temperature, but is intersected by the solidus. Exsolution lamellae in pyroxenes from lunar basalt 12021 are homogenized into the host pyroxene at a temperature close to that of the solidus for a given pyroxene composition. The earliest pyroxenes in rock 12021 crystallized at 1175°C; pyroxene crystallization continued to approximately 960°C.

Introduction

Many pyroxenes from volcanic and intrusive rocks contain a second, exsolved pyroxene phase. This exsolution, submicroscopic in scale, is especially well developed in lunar basalts, which often contain primary host augite and pigeonite that have unmixed pigeonite and augite, respectively. Since pyroxenes crystallize over a wide range of temperatures in basaltic rocks, an understanding of pyroxene crystallization history is of use in understanding the crystallization history of the whole rocks. In order to further understand the subsolidus pyroxene phase relations as they pertain to volcanic rocks, we have undertaken heating experiments on pigeonites and augites from lunar basalt 12021. The experiments involved the stepwise heating and homogenization of clinopyroxenes of various compositions under controlled oxygen pressures. Although the lunar pyroxenes crystallized in a somewhat simpler system than most terrestrial pyroxenes (no water was present to lower the solidus nor was the oxygen fugacity high enough to produce significant amounts of ferric iron), we believe that significant information can be obtained from experiments on lunar pyroxenes which will be applicable to our understanding of the phase

relations of terrestrial pyroxenes and their host rocks. The experiments delineate the augite-pigeonite miscibility gap for Al,Ti bearing clinopyroxenes, the pyroxene phase relations at the beginning of melting, and place limitations on the temperatures at which pyroxenes of different compositions crystallized.

We have determined the phase relations of both clinopyroxenes and orthopyroxenes with compositions near to those of the pyroxene composition plane enstatite-diopside-hedenbergite-ferrosillite. This paper is the first of a series of studies detailing pyroxene phase relations. Work in progress treats the orthopyroxene \rightleftharpoons clinopyroxene (pigeonite) reaction (Ross, Huebner, N. L. Hickling), pyroxene phase diagram topology (Huebner and A. C. Turnock), and natural pyroxene melting relations (Huebner, Ross, and N. L. Hickling). Preliminary results of the present study have been reported by Ross *et al* (1971a,b).

The exact characterization of pyroxenes from lunar basalts is a difficult, complex, and time-consuming task, for often those phases are highly zoned both with respect to chemical composition and to structure type. Fortunately a number of investigators have thoroughly examined pyroxenes from basalt 12021, and we rely heavily on their work in describing the various clinopyroxenes used in our experiments. Particularly we refer the reader to the studies of Boyd and Smith (1971), Bence *et al* (1970, 1971), Papike *et al* (1971), Weill *et al* (1971), Klein *et al* (1971), Walter *et al* (1971), and Dence *et al* (1971).

¹ Publication authorized by the Director, U. S. Geological Survey.

² Present address: Department of Geology and Institute of Meteoritics, University of New Mexico, Albuquerque, New Mexico 87106.

Apollo 12 Basalts and Rock 12021

James and Wright (1972) distinguish three major groups of Apollo 12 basaltic rocks: olivine-pigeonite basalts, ilmenite-bearing basalts, and feldspathic basalts. The only olivine-free basalt of the first type is rock 12021, of immediate interest to us. This rock is porphyritic with phenocrysts of chrome spinel and pigeonite rimmed with augite in a variolitic groundmass consisting of plagioclase (An₈₅₋₉₇), augite, and minor pyroxferroite, silica, and oxides. The observed mode (in wt percent) obtained from our complete mineral separation is: silica, 2 percent; plagioclase (An₉₀), 27 percent; Mg-rich pigeonite (ave. Wo₁₀En₆₁Fs₂₉), 10 percent; Mg-rich augite (ave. Wo₃₃En₄₅Fs₂₂), 13 percent; ferro-pigeonite (ave. Wo₁₅En₄₅Fs₄₀), and moderate to high-iron ferro-augite (ave. Wo₂₆En₂₄Fs₅₀), 41 percent; pyroxferroite, 2 percent; and oxides, sulfides and metal, 5 percent. Chemical analyses of the whole rock, as determined by four different groups of investigators, are given in Table 1. A calculated mode (James and Wright, 1972) based on analysis 3 given in Table 1 is: pyroxene (ave. Wo_{21.6}En_{34.4}Fs_{44.0}), 66.65 percent; plagioclase (ave. An_{88.0}), 27.02 percent; ilmenite, 4.66 percent; apatite, 0.03 percent; SiO₂, 1.08 percent; and glass, 0.61 percent. The excellent agreement for total pyroxene, plagioclase, and opaque phases indicates that little material was lost during the separation.

The sequence of appearance inferred from the textural relations of basalt 12021 is: (1) spinel and pigeonite, (2) Mg-rich augite, (3) plagioclase, ferro-pigeonite, intermediate ferro-augite, ilmenite, (4) iron-rich ferro-augite, pyroxferroite, and (5) silica.

TABLE 1. Chemical Analyses of Apollo 12 Basalt 12021

	(1)	(2)	(3)	(4)	(5)
SiO ₂	47.05	46.2	46.46	46.7	46.5
Al ₂ O ₃	10.97	12.5	10.55	11.1	10.5
FeO	19.04	19.4	19.68	19.1	19.4
MgO	7.08	5.70	7.60	7.38	7.48
CaO	11.34	11.33	11.37	11.5	11.3
Na ₂ O	.29	.29	.35	.30	.30
K ₂ O	.08	.04	.07	.05	.06
TiO ₂	3.74	3.9	3.44	3.45	3.51
P ₂ O ₅	.09	.08	.01	.09	.09
MnO	.25	.24	.26	.27	.27
S	--	<.1	--	--	--
Cr ₂ O ₃	--	.26	.40	.38	.41
Total	99.9	100.0	100.2	100.3	99.8

(1) Engle *et al.* 1971; (2) Klein *et al.*, 1971; (3) Kushiro and Haramura, 1971; (4,5) Cuttitta *et al.*, 1971.

The crystallization sequences for the major phases appearing in basalt 12021 have been investigated experimentally (Table 4) using whole-rock compositions by quenching from various temperatures below the temperature of complete melting. Green *et al.* (1971) observed olivine, pigeonite, and spinel crystallizing on the liquidus at 1155°C and 1 bar. The olivine (Fo₆₆) was consumed by reaction with liquid to precipitate pigeonite at approximately 1140°C. Plagioclase began to crystallize at 1130°C and coprecipitated with clinopyroxene. Ilmenite began to crystallize at 1090°C and the solidus is estimated to be 1050°C. The authors concluded that plagioclase could have begun to crystallize in rock 12021 before rapid crystallization of the groundmass. Biggar *et al.* (1971) obtained somewhat different results: At one bar with $f_{O_2} = 10^{-12.5}$ bar the crystallization sequence was: spinel at temperatures >1180°, followed by "protohypersthene" + pigeonite at 1180°. Plagioclase + augite began to crystallize at 1142°C, then at 1128°C "protohypersthene" reacted to pigeonite. Ilmenite began crystallizing at 1097°C, and the solidus temperature is 1073°C. It is not clear what Biggar *et al.* (1971) mean by "protohypersthene." It is apparently a pyroxene with parallel extinction and low CaO content—probably orthopyroxene. Experimental work (Ross and Huebner, unpublished data) suggests that Mg-rich orthopyroxenes could crystallize at temperatures as high as 1210°C and then react with the liquid in the temperature interval 1200–1170°C to form pigeonite close to the composition Wo₁₀En₆₂Fs₂₈.

It appears that most of the crystallization from the parent melt of rock 12021 took place at or near the lunar surface. The Mg-rich, Ca-poor pigeonite phenocrysts, however, could have formed at some depth prior to eruption. We do not believe that there is any persuasive evidence that these phenocrysts crystallized under high pressure (>5 kbar). The presence of large amounts of aluminum (as much as six wt percent) in the augite certainly cannot be due to high pressure for their zoning and textures indicate rapid growth from a fractionating liquid. We thus assume that all pyroxenes, except perhaps the Mg-rich, Ca-poor pigeonites, crystallized at low pressure (<1 kbar) and at oxygen pressures at or below the iron-wustite buffer curve.

Pyroxenes in Rock 12021—Previous Work

Extensive electron microprobe examinations of large pyroxene phenocrysts (as much as 2 cm in length) in polished thin sections of lunar rock 12021

have been made by Boyd and Smith (1971), Bence *et al* (1971), and Weill *et al* (1971). Generally the phenocryst pyroxenes are zoned so that they reflect the entire pyroxene crystallization history (Bence and Papike, 1972). Individual pyroxene grains from bulk pyroxene grain separates were analyzed by us and show the same range of composition.

The first pyroxene to crystallize forms the phenocryst cores and is Mg-rich pigeonite of nearly constant composition ($Wo_{10}En_{62}Fs_{28}$). The pigeonite cores are always more calcium-rich at their outer boundaries, where they approach the composition $Wo_{15}En_{56}Fs_{29}$. A discontinuous augite mantle usually surrounds the core and varies in composition from $Wo_{32}En_{47}Fs_{21}$ to $Wo_{30}En_{40}Fs_{30}$. A thin band of ferro-pigeonite of the approximate composition $Wo_{15}En_{45}Fs_{39}$ may appear outside this augite mantle (Boyd and Smith, 1971, p. 442). Lastly, ferro-augite is usually found on the very exterior surfaces of the pyroxene phenocrysts and has compositions as iron-rich as $Wo_{23}En_{12}Fs_{65}$ (Boyd and Smith, 1971, p. 442).

This pyroxene crystallization sequence (1) Mg-rich pigeonite; (2) Mg-rich augite and ferro-pigeonite; and (3) ferro-augite, is plotted diagrammatically in Figure 1 and is shown clearly in the pyroxene quadrilateral composition plots of Boyd and Smith (1971, Figs. 1, 2), Weill *et al* (1971, Figs. 3 a-d), and Bence *et al* (1971, Fig. 6). This chemical zoning is sometimes complicated by preferential crystal growth in certain crystallographic directions and development of different compositions behind crystallographically distinct growth faces (sector zoning). For a thorough discussion of sector zoning in lunar basalts similar to 12021 the reader is referred to the study of Hollister *et al* (1971).

In addition to the complex pyroxene zoning found with respect to Ca, Mg, and Fe, there is also complex zoning with respect to the minor components

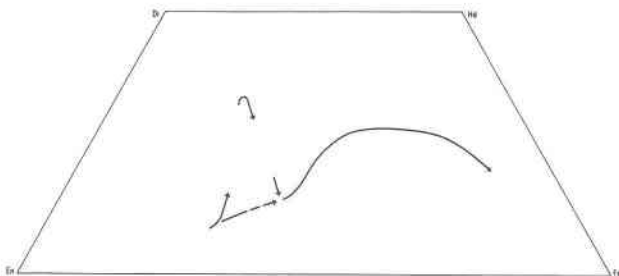


FIG. 1. Pyroxene crystallization trends for lunar rock 12021, deduced from optical, electron microprobe, and X-ray examination of the pyroxenes.

TABLE 2. Bulk Chemical Compositions of Pyroxene Fractions A, B, and C, Lunar Basalt 12021.

	A Mg-pigeonite		B Mg-augite		C Fe-augite	
	wt %	$\frac{\text{cations}^{**}}{6 \text{ oxygens}}$	wt %	$\frac{\text{cations}^{**}}{6 \text{ oxygens}}$	wt %	$\frac{\text{cations}^{**}}{6 \text{ oxygens}}$
SiO ₂	50.1	1.910	48.0	1.852	46.4	1.911
Al ₂ O ₃	1.88	.082	3.97	.177	1.94	.092
FeO	18.0	.561	15.9	.505	29.3	.983
MgO	21.1	1.172	14.4	.814	7.70	.461
CaO	5.57	.222	14.2	.577	11.8	.507
Na ₂ O	0.058	--	0.11	--	0.10	--
K ₂ O	0.086	--	0.11	--	0.12	--
TiO ₂	0.71	.020	1.26	.036	1.20	.036
Cr ₂ O ₃	1.15	.039	1.11	.033	0.10	.002
MnO	(0.35) [†]	.011	(0.35) [†]	.011	(0.35) [†]	.012
Total	99.00		99.41		99.01	
	Mole Percent					
Wo		11.3		30.4		26.0
Fs		28.7		26.6		50.4
En		59.9		42.9		23.6

^{*}Analyst: F. Cuttitta (Dowty *et al*, 1972).

^{**}In deriving the "average" structural formulas shown, silica values obtained by difference were used, and alkalis were ignored. The difference between these formulas and those derived from the numbers shown is not significant.

[†]Manganese was not determined. The values shown are estimates taken from various microprobe analyses (e.g., Bence *et al*, 1970).

Al, Ti, and Cr. For our present purposes, however, we will ignore the effect on clinopyroxene subsolidus phase relations of Al₂O₃, TiO₂, and Cr₂O₃ which, except in extraordinary cases, make up less than 5 wt percent of the pyroxene composition.

Sample Separation and Characterization

Four pyroxene concentrates (A, B, C, and D) were prepared for our present study from rock chips 12021,29 and 12021,103 by crushing to pass 100 mesh, magnetic separation, centrifuging in heavy liquids, and hand picking. Some of the grains from the four fractions may be portions of the large phenocrysts and some are probably groundmass pyroxenes that crystallized contemporaneously with the portions of the phenocrysts that are chemically similar. The pyroxenes from each separate were characterized as to structural state and chemical composition with single crystal X-ray precession photographs, point chemical analyses on representative grains using the electron microprobe, and wet chemical analyses on portions of fractions A, B, and C (Table 2).

The "mode"³ of 10 to 15 crystals from each of the four separates was determined from the single

³ Pyroxenes often unmix one or more phases during subsolidus cooling, thus becoming "multiphase rocks." So the use of the word "mode" is appropriate.

crystal X-ray precession photographs of the $h0l$ and $0kl$ reciprocal lattice nets. Usually 72 hour exposures with molybdenum unfiltered X-radiation were made of each net. Unit-cell parameters for the host and included phases were determined from measurement of the quartz calibrated films. The cell edges are generally accurate to ± 0.2 percent and angles to $\pm 0.1^\circ$. The relative amounts of host, exsolved, and epitaxially overgrown pyroxenes were estimated by visually comparing the intensities of the $h0l$ reflections having identical index, because the scale of exsolution is too fine to be detected by optical or microprobe methods. Such procedures were first used by Ross *et al* (1969) in their study of exsolution in amphiboles. The $h0l$ diffraction patterns of typical low calcium and high calcium Mg-rich pigeonites which compose fraction A are shown in Figure 2A and 2B. Typical Mg-rich augite (fraction B) and ferro-augite (fraction C) patterns are shown in Figure 2C and 2D.

Electron micrographs taken by E. J. Dwornik (U.S.G.S.) of our fraction A and B clinopyroxenes and those of Fernandez-Moran *et al* (1971) of

pyroxenes from a chip of the same lunar basalt show exsolution lamellae only a few hundred angstroms thick. With the optical microscope we observed only one grain with visible exsolution lamellae. Due to the very small size and generally even distribution of the exsolution lamellae as shown by these electron microscope studies, the chemical compositions as determined by the electron microprobe over a 2 to 5 micron region are believed to represent closely the average or *bulk* compositions which existed prior to exsolution.

Fraction A is composed entirely of Mg-rich pigeonite crystals 0.05 to 0.5 mm long, euhedral to subhedral, and often showing prominent $\{110\}$ cleavage forms and occasionally $\{100\}$ and $\{010\}$ forms. There is very little visible evidence of any epitaxial overgrowth of the more reddish augite which is seen mantling the large pyroxene phenocrysts. Ninety-five percent or more of the pigeonites in fraction A have a low calcium content ($W_{O_{8-11}}$); a few grains were found to have a higher calcium content ($W_{O_{11-15}}$). The bulk grain compositions as determined by repeated electron probe analyses on

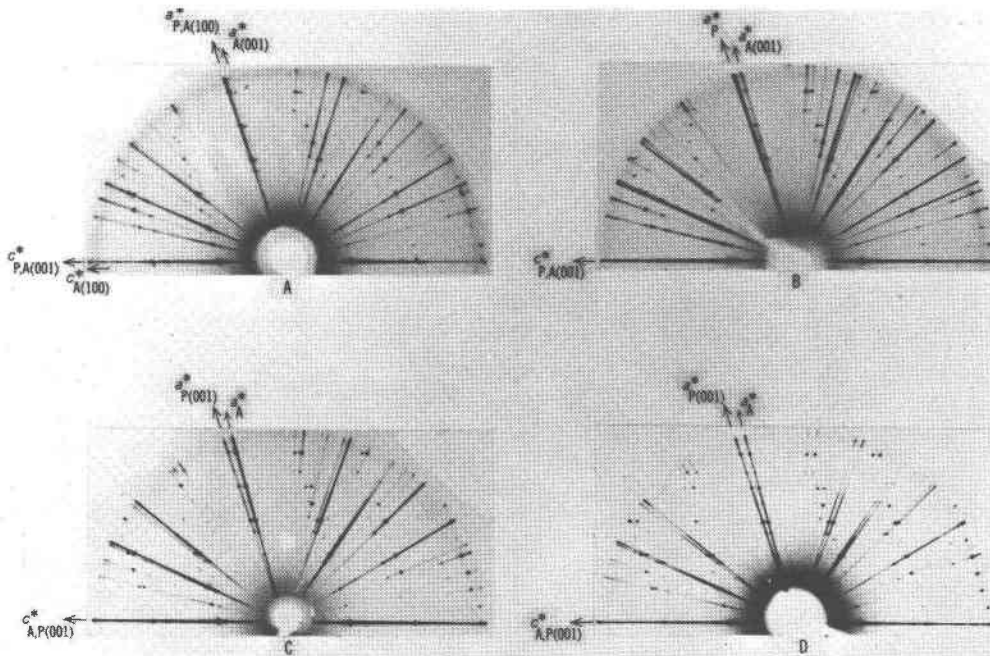


FIG. 2. $h0l$ precession photographs ($MoK\alpha$, unfiltered X-radiation) of (A) low-calcium Mg-rich pigeonite fraction A containing 10 percent augite oriented on (001) and 2 percent augite oriented on (100); (B) high-calcium, Mg-rich pigeonite from fraction A containing 35 percent augite on (001); (C) Mg-rich augite from fraction B containing 35 percent pigeonite on (001); and (D) ferro-augite containing 50 percent ferro-pigeonite on (001). The reciprocal axes a^* and c^* are designated as follows: P-pigeonite host, A-augite host, A(100)-augite on (100), A(001)-augite on (001), P(001)-pigeonite on (001).

several low calcium grains varies slightly, from $Wo_{8 \text{ to } 11}$, $En_{59 \text{ to } 63}$, and $Fs_{28 \text{ to } 31}$. The average composition represented by probe analyses of low-Ca grains is $Wo_{10}En_{61}Fs_{29}$ (Fig. 3). Wet chemical analysis of a 50-mg portion of fraction A gives the average composition of $Wo_{11.3}En_{59.9}Fs_{28.7}$ (Table 2) for the aggregate of fraction A pigeonites. These compositions are in good agreement with composition of core pigeonite in large phenocrysts analyzed by Boyd and Smith (1971), Weill *et al* (1971), and Bence *et al* (1971), which are, respectively, $Wo_{12}En_{61}Fs_{27}$, $Wo_{10}En_{62}Fs_{28}$, and $Wo_9En_{63}Fs_{28}$. Some of the low calcium pigeonite crystals examined by us zone to slightly more calcium-rich compositions, approaching an apparent limit of about $Wo_{15}En_{55}Fs_{30}$. The phenocryst cores also show this type of zoning, particularly in the "(100) sector" (Boyd and Smith, 1971, Fig. 2). The high-calcium pigeonite grains from fraction A have bulk compositions that are similar to that of the grain margins of the low calcium pigeonites.

X-ray precession photographs show that calcium-poor pigeonites contain 5 to 10 percent exsolved augite oriented on (001) and 1 to 2 percent exsolved augite oriented on (100). Calcium-rich pigeonite grains contain 20 to 35 percent augite oriented only on (001).

Electron probe analyses of the Mg-rich augite composing fraction B show that there is a preferential grouping in the compositional range Wo_{29-38} , En_{43-49} , and Fs_{20-24} , averaging $Wo_{33}En_{45}Fs_{22}$ (Fig. 3). Wet chemical analysis of a 50 mg portion of fraction B (Table 2) gives an average composition of $Wo_{30.4}En_{42.9}Fs_{26.6}$, suggesting that the selection of grains for probe analysis was somewhat biased⁴ to the more Mg-rich augites. Crystals from fraction B are equivalent to the augite, forming the inner part of the phenocryst mantle in contact with the pigeonite core described by Boyd and Smith (1971, p. 442) as having the composition $Wo_{32}En_{46}Fs_{21}$. X-ray photographs of fraction B augite indicate that they contain approximately 35 percent exsolved pigeonite in (001) orientation. Electron-microprobe analyses and the X-ray photographs indicate that there is little or no zoning to more Fe-rich compositions (Fig. 3) and little epitaxial overgrowth of ferro-pigeonite in the fraction B augites.

Fraction C is composed of more highly zoned

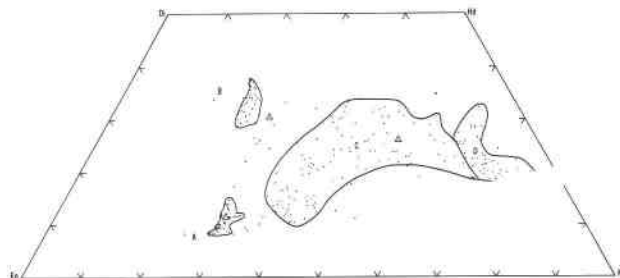


FIG. 3. Distribution of 278 microprobe spot analyses on grains selected from lunar rock 12021 pyroxene separates made for this study. Wet chemical analyses (Table 2) are also shown by Δ . The comparison between wet chemical and microprobe analyses is discussed in the text.

clinopyroxenes and includes ferro-pigeonite (approximate composition, $Wo_{15}En_{45}Fs_{40}$) and intermediate ferro-augite (Fig. 3). The ferro-pigeonite grains appear to correspond genetically to the "pigeonite band in the phenocryst mantle" reported by Boyd and Smith (1971, p. 442; see also Bence *et al* 1971) as having the composition $Wo_{15}En_{45}Fs_{39}$. X-ray photographs show that the ferro-pigeonite host contains about 35 percent exsolved augite oriented on (001) and that the intermediate ferro-augite host invariably contains 50 percent exsolved ferro-pigeonite oriented on (001).

It is in the clinopyroxenes from fraction C that we see clear evidence of epitaxial overgrowth of one clinopyroxene on another. The best example of epitaxy is seen in grain 13D from fraction C which consists of ferro-pigeonite of average composition $Wo_{13}En_{45}Fs_{10}$ epitaxially overgrown by ferro-augite of average composition $Wo_{23}En_{40}Fs_{37}$. Eighteen electron probe analyses made over the polished surface of the grain clearly delineate the pigeonite-augite overgrowth boundary, shown as a dashed line in Figure 4A. These analyses are plotted within a portion of the pyroxene quadrilateral in Figure 4B.

The intensities of the X-ray reflections displayed in the precession photographs of grain 13D show that it was originally composed of approximately 80 percent host pigeonite and 20 percent host augite; the ratio of the two host phases (4.0) corresponding well (considering the difficulty in estimating the crystal "mode") to the apparent ratio (2.9) obtained from multi-point electron probe analysis (Fig. 4A). The host pigeonite (a 9.714, b 8.937, c 5.232Å, β 108.68°) now contains about 20 percent augite (a 9.709, b 8.937, c 5.266Å, β 106.08°) exsolved on (001). The host augite (a 9.733, b

⁴Only the most optically homogeneous, clear yellow augite grains were selected for microprobe analysis.

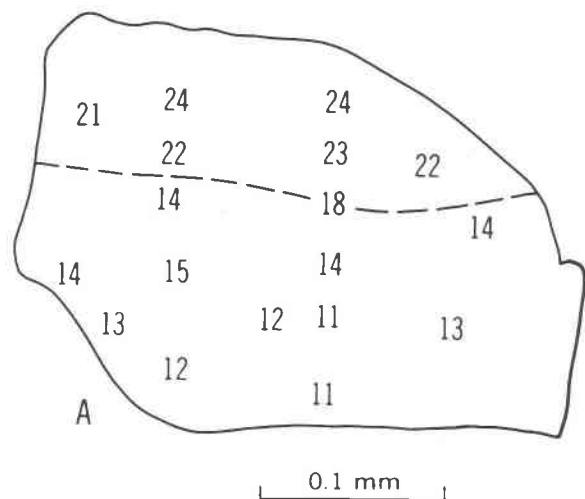
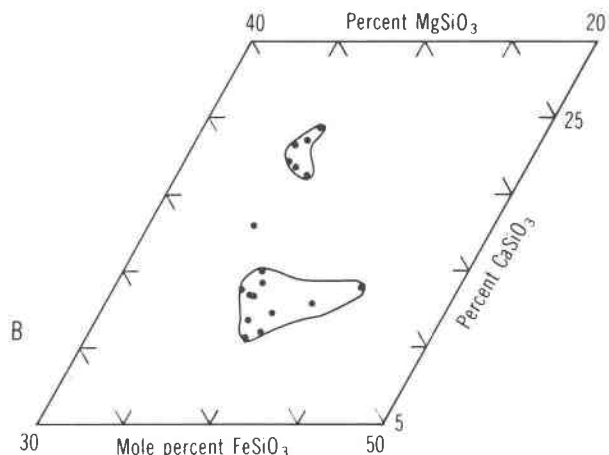


FIG. 4A. Sketch of polished surface of grain 13D showing Wo mole percent values determined at 18 locations by microprobe analyses. Note the presence of a sharp boundary between pigeonite (Wo 11–15) and augite (Wo 21–24).

8.937, c 5.265Å, β 105.98°) now contains about 50 percent pigeonite (a 9.741, b 8.937, c 5.229Å, β 108.85°) exsolved on (001). The present mode of the grain is: host pigeonite—64 percent, host augite—10 percent, (001) pigeonite—10 percent, and (001) augite—16 percent.

Clinopyroxene grains in which there is an epitaxial overgrowth of a second clinopyroxene such as that described above have X-ray patterns that differ from those of clinopyroxenes in exsolution intergrowth. In composite grains the two clinopyroxenes, augite and pigeonite, share a common b -direction. However, neither the a nor the c axes of the two phases are parallel but deviate from one another by approximately $1^{\circ}15'$, a value very close to $\Delta\beta/2$, where $\Delta\beta = \beta_{\text{pigeonite}} - \beta_{\text{augite}}$. The axial relationships within the (010) plane of such a pigeonite-augite overgrowth are shown diagrammatically in Figure 5. This type of overgrowth is easily distinguished in lunar pyroxenes from (001) and (100) exsolution intergrowths, for in exsolution intergrowth the a or the c axes of the co-existing pair are always parallel within a few minutes arc.

The densest fraction (D) is composed of very iron-rich augite and corresponds to Boyd and Smith's (1971, p. 442) "outer mantle" ferro-augite for which they report a composition of $\text{Wo}_{23}\text{En}_{12}\text{Fs}_{65}$ (Fig. 3). Augite grains in this fraction also invariably contain 50 percent pigeonite unmixed on (001). Epitaxial overgrowths of iron-rich pigeonite are generally not seen in grains from this fraction.



4B. The same 18 points plotted on part of the pyroxene quadrilateral.

Experimental

X-ray examination

Small crystals, 0.1 to 0.3 mm in length, were selected from the various fractions for single crystal X-ray study. The crystals that gave well resolved and sharp X-ray reflections were then used in the

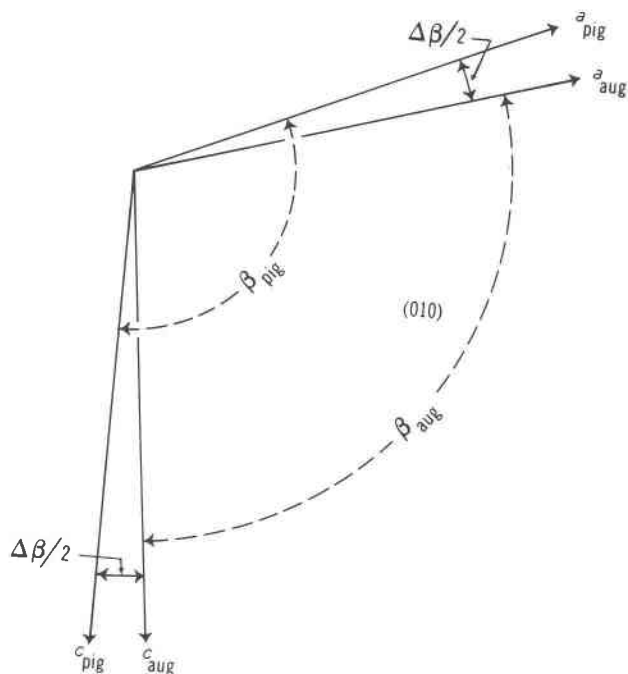


FIG. 5. Sketch of the axial relations within the common (010) planes of epitaxially related augite and pigeonite, crystal 13D. The sketch exaggerates the value of $\Delta\beta$, actually $\Delta\beta = \beta_{\text{pig}} - \beta_{\text{aug}} = 1.25^{\circ}$.

subsequent heating experiments. Such crystals show restricted chemical zoning and very little epitaxial overgrowth of a second clinopyroxene as indicated by well defined temperatures of homogenization, by electron microprobe analysis, and by X-ray analysis. In all 24 crystals were used in these experiments.

After the initial X-ray examination the single crystals were heated, quenched, and again X rayed. Complete unit-cell parameters for both host and exsolved phases were then obtained from $h0l$ and $0kl$ photographs. The same crystals were then returned to the furnace for the next heating step and the whole process repeated for as many as nine heating cycles.

The change in the unit-cell parameters and the change in the relative X-ray intensities of the host and exsolved clinopyroxene describe the amount of exsolved phase that has dissolved back into the host at any particular heating temperature. The "beta" (β) angle is particularly sensitive to changes in the calcium content of both augite and pigeonite (Papike *et al*, 1971; Turnock *et al*, 1973) and is thus very useful in delineating a section of the augite-pigeonite solvus; however, absolute Wo values are not well known from the present b - β plots.

Heat treatment

Heating experiments were conducted in a vertically mounted, platinum wound quenching-style furnace. The temperature variation in the hot zone was $\pm 1^\circ\text{C}$ over 1 cm and $\pm 3^\circ\text{C}$ over 3 cm. Temperature was measured with Pt-Pt₉₀Rh₁₀ thermocouples sheathed by enclosure with an oxygen "probe" (see below). The temperature range of interest is 900°C – 1200°C ; the thermocouples were calibrated against gold (melting point 1064.4°C , IPTS '68) enclosed in glass capsules suspended in the sample position. The uncertainty in bracketing the gold melting point was $\pm 1^\circ\text{C}$. Thermocouple EMF was recorded continually on one channel of a two-pen strip chart recorder; with a 20 mV full-scale range, the uncertainty (expressed as temperature) due to reading of the chart is less than $\pm 2^\circ\text{C}$. Recorded temperature variation during a run was commonly less than 3°C . Overall temperature uncertainty is estimated to be within $\pm 7^\circ\text{C}$. Run data are summarized in Table 3.

Runs designated EST (Table 3) were made in evacuated silica tubes at the beginning of this investigation. Pyroxene crystals were individually wrapped in Pt foil packets, and one or more packets were

sealed in an evacuated silica tube. The tubes were hung in the hot zone of the furnace in air or CO_2 . The air pressure in the vacuum line was monitored during the sealing of the tube; calculation of conditions within the tube at the run temperature indicates that the oxygen fugacity was such that magnetite would be the stable iron oxide phase. Quench crystals were examined for evidence of oxidation—oxides on surface of grain, dusty inclusions, or reddish discoloration—but none was found. However, precession photographs of crystals heated in evacuated silica tubes commonly showed a weak, spotty ring pattern of cristobalite. In the absence of direct evidence for oxidation, we believe the source of this cristobalite is the silica tube itself. In a successful effort to avoid silica contamination, we conducted later series of experiments in which crystals were exposed directly to a reducing furnace atmosphere. In none of these runs was cristobalite ever identified, only rare occurrences of tridymite (see crystals 2D and 26D in Table 3). This tridymite could conceivably be part of the lunar rock 12021 mesostasis that is attached to the crystals, yet overlooked during selection of the crystals.

Runs designated OFA in Table 3 were equilibrated with a furnace atmosphere of mixed CO_2 and H_2 . At T , P , and equilibrium, the oxygen fugacity of this gas mixture is proportional to the initial mixing ratio $P_{\text{CO}_2}/P_{\text{H}_2}$ (Nafziger *et al*, 1971). The flow rates of CO_2 and H_2 were individually regulated by a gas apparatus train (Fig. 6) consisting of pressure regulators, capillaries, and valves. The gas pressure regulators maintain a constant pressure (1–3 psi) on the upstream side of a minute orifice (capillary or low flow rate valve). Gas is permitted to "leak" through the orifice. A flow rate may be changed by varying a gas pressure "head" or the size of an orifice; mixing ratios of 1000:1 can be obtained at low flow rates with a single mixing stage. The nominal flow rate was approximately six liters per hour checked with a ball-type flowmeter calibrated for air at NPT, yet used for the input or exhaust gases. Equivalent flow rates in the furnace (16 mm diameter) are 0.94 cm/sec (next to the oxygen cell) and 0.80 cm/sec above the oxygen cell. This range of flow rate corresponds well with the 0.9 cm/sec recommended by Darken and Gurry (1945) as being satisfactory for this kind of work. This simple and inexpensive equipment is sufficient to maintain a $P_{\text{CO}_2}/P_{\text{H}_2}$ so constant that the f_{O_2} of a furnace atmosphere varies less than 0.1 log atm unit over a week's duration.

TABLE 3. Results of Pyroxene Heating Experiments: Run Conditions, Cell Data, Crystal Modes*

Temp. (°C)	Hours	Host Pigeonite, fraction A				(001) Augite				Percent augite	Phases detected	Run type
		a, Å	b, Å	c, Å	β°	a, Å	b, Å	c, Å	β°			
(Crystal 3R)												
25°		9.684	8.903	5.207	108.67	9.674	8.903	5.261	105.97	30	AP	
950	90	9.710	8.910	5.222	108.67	9.689	8.910	5.279	106.07	30	AP	EST
1164	19	9.705	8.900	5.241	108.38	9.705	8.900	5.261	107.07	15	APC	EST
1211	19	9.707	8.879	5.250	108.33	9.707	8.878	5.238	106.50	10	APC	EST
1228	21	9.681	8.889	5.254	108.53	9.690	8.889	5.241	106.50	35	APC	EST
1243	22	9.679	8.891	5.200	108.50	9.727	8.891	5.232	106.47	50	APC	EST
1262	21	9.694	8.861	5.226	108.52	9.740	8.861	5.259	106.58	50	APCG	OFA
1274	21	9.661	8.868	5.209	108.43	9.716	8.868	5.244	106.52	50	APG	OFA
(Crystal 1R)												
25		9.692	8.911	5.218	108.67	9.677	8.907	5.281	106.00	30	AP	
1063	41	9.704	8.916	5.238	108.67	9.697	8.916	5.263	106.46	30	AP	EST
1148	19	9.712	8.913	5.252	108.47	9.712	8.913	5.264	106.87	20	AP	EST
1177	24	9.712	8.912	5.264	108.27	9.712	8.912	5.256	107.03	9	APC	EST
1184	31	9.724	8.920	5.264	108.32	9.703	8.920	5.296	106.92	5	APCH	EST
1208	20	9.715	8.904	5.258	108.37	9.666	8.904	5.230	106.45	5	APC	EST
(Crystal 3D)												
25		9.705	8.911	5.234	108.88	9.708	8.911	5.273	106.08	35	AP	
1176	19	9.720	8.931	5.266	108.25					0	P	EST
1208	20	9.702	--	5.236	108.65	9.702	--	5.250	106.70	35	APG?	EST
1258	29	9.693	8.918	5.226	108.47	9.693	8.918	5.260	106.53	70	APG	EST
(Crystal 18R)												
25		9.694	8.898	5.208	108.70	9.675	8.898	5.280	105.97	20	AP	
1029	69	9.694	8.903	5.220	108.65	9.694	8.903	5.268	106.35	15	AP	OFA
1059	115	9.694	8.899	5.232	108.58	9.694	8.899	5.268	106.43	15	AP	OFA
1089	92	9.681	8.892	5.237	108.58	9.681	8.892	5.277	106.58	10	APH	OFA
1128	95	9.705	8.904	5.244	108.42	9.705	8.904	5.253	106.47	5	APH	OFA
971	67	--	--	--	108.50	--	--	--	106.33	5	APH	OFA
1050	289	9.690	--	5.231	108.53	9.690	--	5.276	106.42	15	APH	OFA
Temp. (°C)	Hours	Host Augite, fraction B				(001) Pigeonite				Percent pigeon.	Phases detected	Run type
		a, Å	b, Å	c, Å	β°	a, Å	b, Å	c, Å	β°			
(Crystal 1D)												
25		9.712	8.894	5.270	106.05	9.699	8.894	5.220	108.78	45	AP	
1064	66	9.706	8.906	5.266	106.37	9.720	8.906	5.234	108.60	40	AP	EST
1176	19	9.726	8.911	5.264	107.27					0	A	EST
		9.726	8.911	5.256	106.00							
1211	19	9.731	8.926	5.273	107.40						A	EST
		9.731	8.926	5.259	106.30							
1228	21	9.720	8.864	5.243	106.72					0	AG	EST
1243	18	9.734	8.918	5.252	106.77					0	AG	EST
		9.734	8.918	5.252	106.08							
1258	29	9.726	8.910	5.245	106.00					0	AG	EST
(Crystal 14R)												
25		9.729	8.907	5.274	106.07	9.708	8.907	5.226	108.88	50	AP	
1050	95	9.733	8.912	5.256	106.42	9.733	8.912	5.242	108.50	50	AP	OFA
1091	44	9.712	8.914	5.279	106.55	9.712	8.914	5.254	108.48	50	AP	OFA
1114	71	9.721	8.913	5.264	106.65	9.712	8.913	5.256	108.40	50	AP	OFA
1136	39	9.731	8.916	5.272	106.83	9.713	8.916	5.264	108.35	40	APG	OFA
1148	47	9.720	8.916	5.251	106.87	9.720	8.916	5.276	108.26	20	AP	OFA
1168	18	9.720	8.908	5.253	107.07	--	8.908	5.244	108.55	5	APG	OFA
(Crystal 17D)												
25	67	9.738	8.909	5.261	106.15	9.738	8.909	5.213	108.83	35	AP	
1142	21	9.748	8.921	5.260	106.80					0	APH	OFA

*Notes. Phases detected: P-pigeonite, A-augite, C-cristobalite, T-tridymite, G-glass, H-holocrystalline (glass sought, not found).
Run type: OFA - open to furnace atmosphere, EST - evacuated silica tubes.

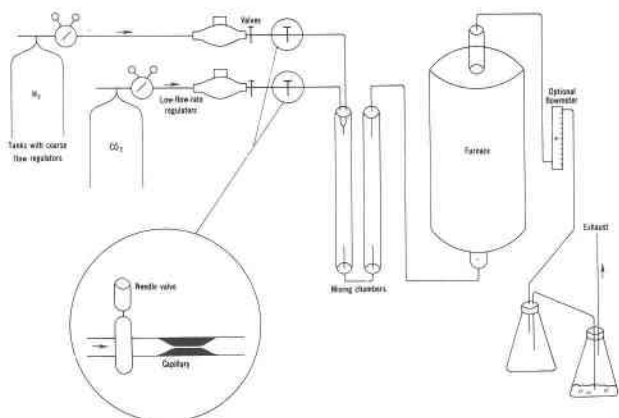


Fig. 6. Simplified diagram of the gas train used to maintain a constant, predetermined oxygen fugacity in the furnace.

Oxygen fugacity was measured directly in the hot spot of the furnace, adjacent to the samples, using the calcia-stabilized zirconia electrolyte cell.

Reference Gas (O₂), Pt [(Zr_{0.85}Ca_{0.15})O₂] Pt, Furnace Gas

Sato (1971) reviews the use of such devices. Elements of the cell are shown by Sato (1970, Fig. 1), but details of construction used here differ. Cell EMF was monitored continuously on the second channel of a two-pen recorder. The uncertainties of electrochemical oxygen fugacity determinations themselves have been discussed by Huebner and Sato (1970). The direct f_{O_2} measurement obviates the uncertainties (mixing ratio, gas flow and reaction

TABLE 3, Continued

Temp. (°C)	Hours	Host Augite, fraction B				(001) Pigeonite				Percent pigeon.	Phases detected	Run type
		a, Å	b, Å	c, Å	β°	a, Å	b, Å	c, Å	β°			
(Crystal 19D)												
25		9.744	8.901	5.260	106.25	9.744	8.901	5.221	108.83	30	AP	
1142	67	9.738	8.928	5.272	106.72	9.738	8.928	5.255	108.35	5	APH	OFA
1161	46	9.717	8.916	5.263	106.72	9.766	8.916	--	108.12	2	APH	OFA
1089	92	9.730	8.915	5.253	106.70	9.734	8.915	--	108.45	5	APH	OFA
(Crystal 8D)												
25		9.720	8.912	5.271	106.13	9.720	8.912	5.207	108.87	35	AP	
1002	65	9.733	8.932	5.263	106.27	9.733	8.932	5.236	108.70	35	APC	EST
1048	46	9.718	--	5.268	106.32	9.718	--	5.246	108.68	30	AP	EST
1107	20	9.724	8.916	5.256	106.40	9.724	8.916	5.238	108.37	25	AP	EST
1149	18	9.727	8.924	5.262	106.95	9.727	8.924	5.257	108.25	5	AP	EST
		9.727	8.924	5.252	105.95							
1175	42	9.742	8.916	5.276	106.93					0	A	EST
		9.742	8.916	5.276	106.00							
(Crystal 10D)												
25		9.745	8.918	5.266	106.26	9.745	8.918	5.222	108.88	25	AP	
1050	95	9.731	8.930	5.252	106.58	9.731	8.930	5.244	108.57	20	AP	OFA
1091	44	9.732	8.917	5.265	106.66	9.732	8.917	5.252	108.42	10	AP	OFA
1114	71	9.734	8.914	5.262	106.72					trace	AP	OFA
1129	44	9.730	8.911	5.259	106.80					trace	APH	OFA
1161	46	9.727	8.926	5.263	106.80					trace	APH	OFA
		--	--	--	106.10							
Temp. (°C)	Hours	Host Augite, fraction C				(001) Pigeonite				Percent pigeon.	Phases detected	Run type
a, Å	b, Å	c, Å	β°	a, Å	b, Å	c, Å	β°					
(Crystal 2D)												
25		9.718	8.993	5.262	105.93	9.718	8.993	5.258	108.77	50	AP	
1050	95	9.762	8.999	5.255	106.97	9.774	8.999	5.275	107.73	3	APT	OFA
		9.720	8.999	5.233	106.13							
1091	44	9.761	8.977	5.256	106.52					trace	APT	OFA
		9.744	8.977	5.245	106.12							
1114	71	9.767	8.958	5.266	106.03					0	AT	OFA
1142	67	9.760	8.957	5.264	106.05					0	ATG	OFA
(Crystal 5D)												
25		9.783	9.017	5.269	105.97	9.785	9.017	5.257	108.67	40	AP	
899	42	9.768	--	5.263	106.02	9.768	--	5.259	108.53	40	AP	OFA
952	39	9.765	--	5.266	106.13	9.765	--	5.258	108.30	35	AP	OFA
1002	43	9.769	8.994	5.250	106.43	9.769	8.994	5.263	108.00	20	AP	OFA
1029	69	9.757	8.992	5.256	106.75	9.757	8.992	5.274	107.83	5	APH	OFA
		9.720	8.992	--	106.02							
844	238	9.763	8.977	5.260	106.57	9.763	8.971	5.259	108.33	10	APH	OFA
Temp.	Hours	Host Augite, fraction D				(001) Pigeonite				Percent pigeon.	Phases detected	Run type
a, Å	b, Å	c, Å	β°	a, Å	b, Å	c, Å	β°					
(Crystal 19R)												
25		9.740	9.028	5.254	105.73	9.740	9.028	5.258	108.60	50	AP	
853	46	9.757	9.027	5.259	105.83	9.757	9.027	5.262	108.43	50	AP	OFA
898	120	9.768	9.023	5.253	106.02	9.768	9.023	5.267	108.17	50	AP	OFA
949	118	9.776	9.024	5.255	106.50	9.776	9.024	5.267	107.78	40	AP	OFA
960	138	9.770	9.021	5.258	106.75	9.770	9.021	5.270	107.62	20	APG?	OFA
		9.770	9.021	5.262	106.00							
(Crystal 26D)												
25		9.752	9.017	5.249	105.57	9.752	9.017	5.251	108.43	50	AP	
853	46	9.760	9.010	5.255	105.85	9.760	9.010	5.263	108.40	50	AP	OFA
898	120	9.773	9.011	5.245	105.95	9.773	9.011	5.252	108.08	50	AP	OFA
949	118	9.765	9.006	5.249	106.30	9.765	9.006	5.262	107.83	40	APT	OFA
962	93	9.742	9.023	5.246	106.35	9.742	9.023	5.265	107.67	35	APG	OFA
971	67	9.778	9.020	5.243	106.65	--	9.023	5.269	107.63	30	APG	OFA

*Notes. Phases detected: P-pigeonite, A-augite, C-cristobalite, T-tridymite, G-glass, H-holocrystalline (glass sought, not found).
Run type: OFA - open to furnace atmosphere, EST - evacuated silica tubes.

rates, impurities, leaks into or out of the gas stream) associated with the traditional calibrated gas-mixer methods. This apparatus will measure oxygen fugacity in the desired f_{O_2} range, that is, several tenths of a log atm unit below that of the iron-wustite assemblage, to at least 0.05 log atm unit.

Most heating experiments lasted 15–200 hours; several experiments were much longer. A homogenization step was judged to be essentially completed during an overnight run because repeated heatings at the same temperature did not result in observed additional homogenization. At the termination of an experiment, a sample was removed from the furnace

and quenched in mercury. The platinum foil sample container of an OFA run (Table 3) was cooled to room temperature within one second after removal from the furnace hot zone; due to the thermal insulation afforded by silica tubing, EST runs were quenched to room temperature more slowly, probably within several seconds. Experiments described below show that the rate of growth of exsolution lamellae is so slow that detectable back-reaction could not have occurred during any quench.

Single crystals for OFA runs were wrapped in platinum foil, selected because of its high melting point and the fact that the outer electrode of the

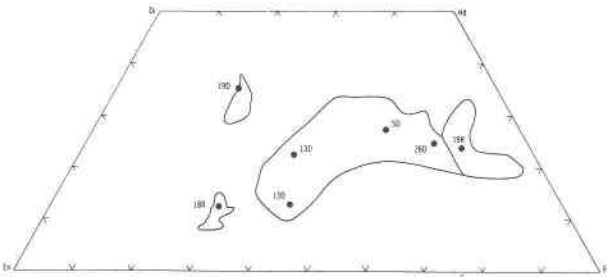
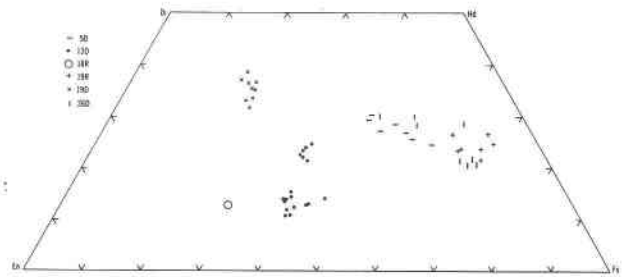


FIG. 7A. Microprobe analyses of heated (but unmelted) crystals plot within the compositional range of the fractions A, B, or C from which the crystals were selected, indicating no appreciable loss of iron to the platinum foil containers. Analyses by A. E. Bence and by Huebner.



7B. Plot of microprobe spot analyses for five of the clinopyroxene crystals used in the heating studies (see Figs. 9 and 10) and for crystal 13D (Fig. 4A, B). Analysts, A. E. Bence and J. S. Huebner.

oxygen cell was also platinum. We looked for, but did not observe, evidence of iron loss from clinopyroxene in the *subsidius* experiments reported here, or from seven orthopyroxenes in other experiments (unpublished data). Such evidence would be the presence of a silica phase, change in unit-cell dimension⁵, or a depletion of the FeSiO_3 component in the grain as determined by microprobe. The chemical evidence for constancy of clinopyroxene bulk composition is shown in Figure 7; the analyses of heated crystals plot within the respective fields defined by the compositional groups from which they were chosen. We will show in a later paper that, after appreciable liquid is formed and comes in contact with the platinum, iron is rapidly lost from both liquid and crystal.

We chose an oxygen fugacity several tenths of a log atm unit of f_{O_2} below that of the assemblage $\text{Fe} + \text{Fe}_{1-x}\text{O}$ in order to avoid decomposing the pyroxene (by oxidation or reduction) and to approximate the oxygen fugacity of the lunar environment in which the pyroxene single crystals formed. At the time we initiated the study, the crystallization history of the Apollo 12 samples had not been thoroughly investigated. However, many investigators had indicated the exceedingly reduced nature of the Apollo 11 basalts, and by analogy, we selected similarly reducing conditions. Subsequent work, including the discovery of nearly pure iron metal in both pyroxene and groundmass of basalt 12021 (Walter *et al.*, 1971; Weill *et al.*, 1971), attests to the reducing environment of crystallization for Apollo 12 basalts.

⁵ The b dimension of clinopyroxene is a sensitive indicator of changes in $\text{Fe}/\text{Mg}+\text{Fe}$; a change in this ratio of 0.25, corresponds to a change of approximately 0.1Å in the b dimension.

Results

Run conditions and data pertinent to phase characterizations are summarized in Table 3 and Figure 9. Heating experiments for each crystal are arranged (Table 3) top to bottom in the order in which the experiments were actually performed. Experiments in which we attempted to reverse the homogenization process are apparent because the temperature first increases, then decreases as listed in the table. Methods used to determine the parameters listed in Table 3 are described below.

Precession photographs of the $h0l$ net of a typical Ca-rich pigeonite crystal from fraction A, taken before and after various heat treatments, are shown in Figure 8. The a^* axes of host pigeonite and exsolved (001) augite move closer together ($\Delta\beta = \beta_{\text{Pig}} - \beta_{\text{Aug}}$ decreases) with increasing temperature, indicating that the calcium contents of the two phases approach one another. During melting, augite and pigeonite a^* axes again separate, indicating increasing differences in the calcium content of the two phases. In addition to (001) augite, a small amount of augite oriented on (100) is present in some low-calcium fraction A pigeonites. We made no attempt to record the cell dimensions of this augite because of the weakness of the reflections and their early disappearance in the heating sequence.

The β angles of coexisting augite and pigeonite vary regularly with the temperature of a homogenization experiment. The β angle is dependent on the Wo content of pyroxene, but relatively independent of En/Fs (Turnock *et al.*, 1973). Changes in β are a sensitive indicator of changes in the mole percent Wo of a pyroxene, but there is a relatively great uncertainty in assigning a specific percent Wo to a particular value of β , due to the lack of good standards. We have made an estimate by considering

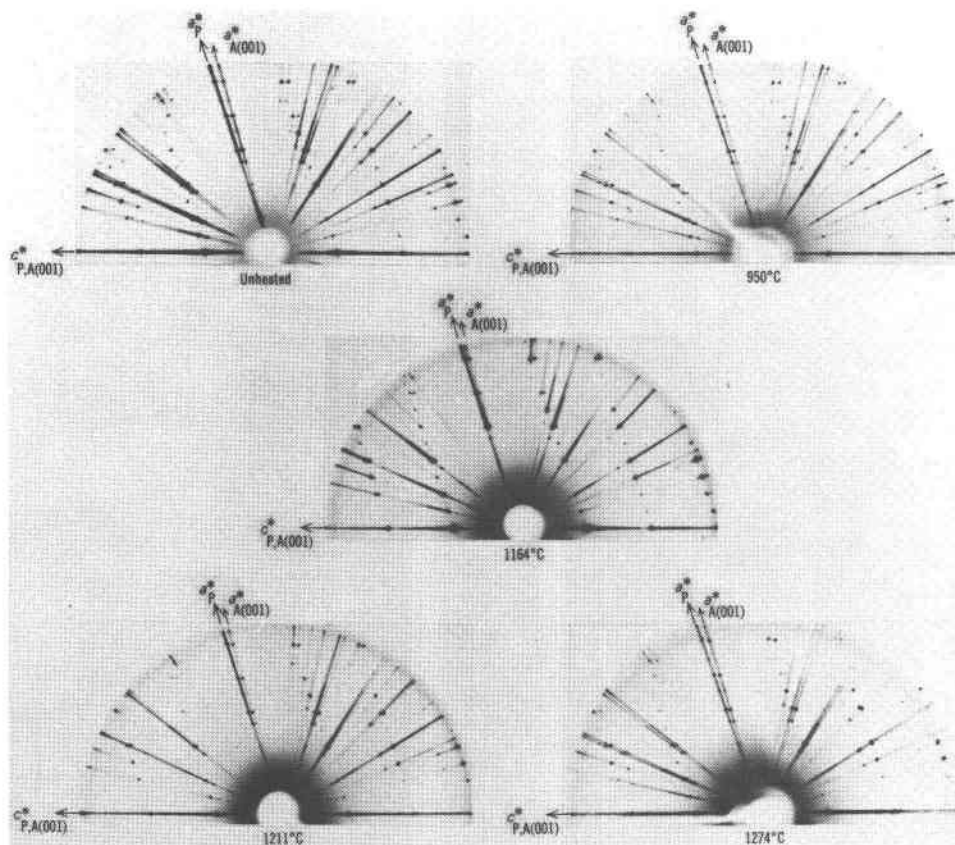


FIG. 8. $h0l$ precession photographs ($\text{MoK}\alpha$, unfiltered X-radiation) of Ca-rich pigeonite crystal 3R originally containing about 30 percent augite exsolved on (001). Photographs taken before heating and after heating to 950°, 1164°, 1211°, and 1274°C — a^* and c^* axes are designated as in Figure 2.

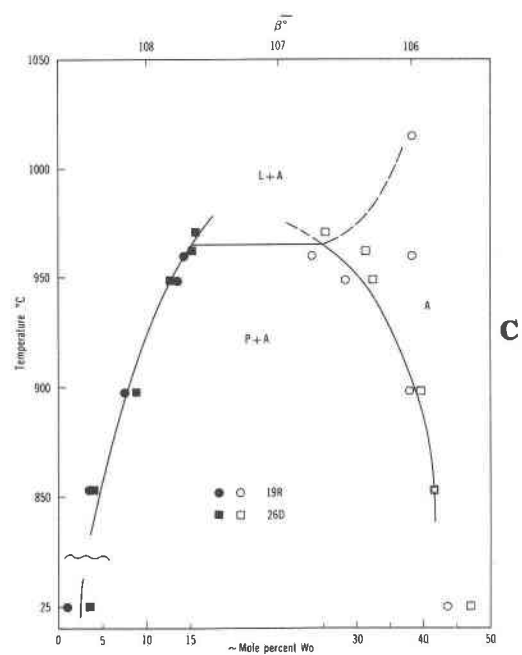
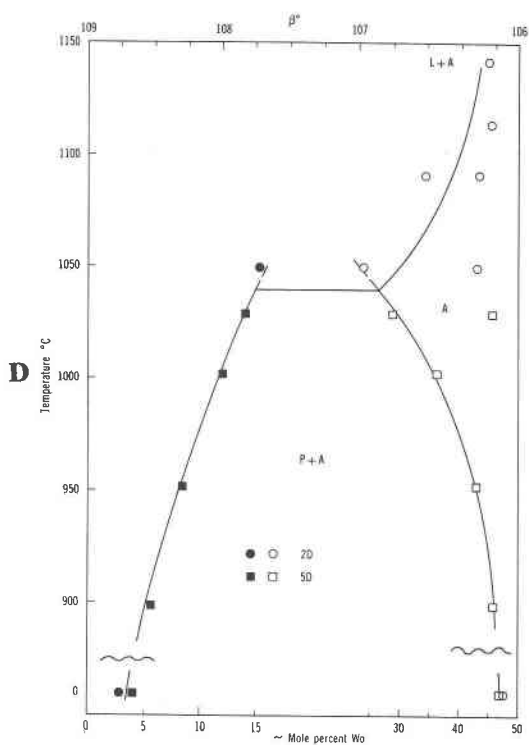
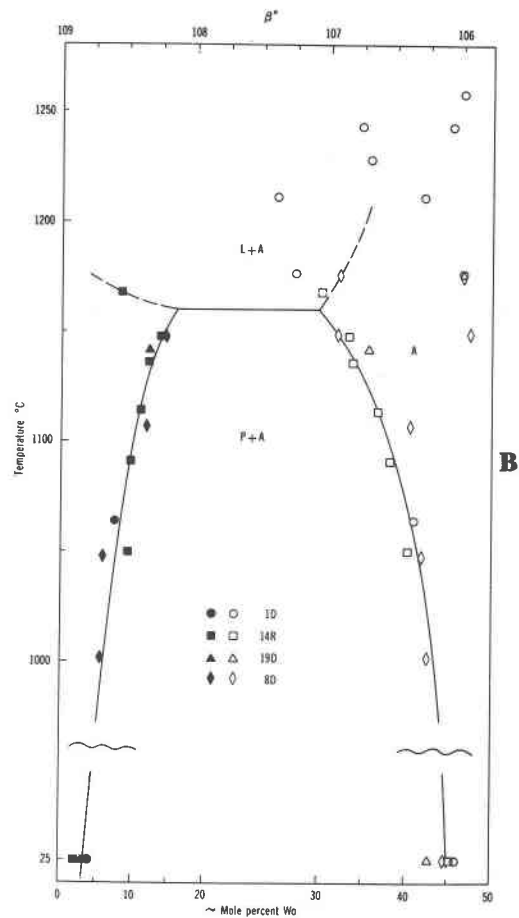
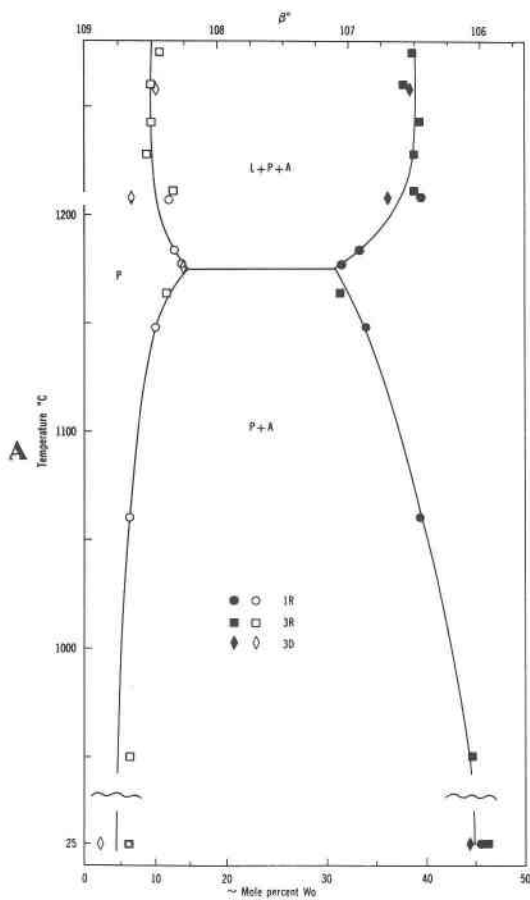
the β angles, bulk compositions, and proportions of phases in unheated grains, and the β angles at which these grains become homogenized, but at present the precision greatly exceeds the accuracy of the method. However, it is clear that with increasing temperature, $\Delta\beta$ decreases, corresponding to a narrowing of the augite-pigeonite miscibility gap.

The b of a clinopyroxene varies greatly with En/Fs, but is relatively insensitive to variations in Wo content except for very En-rich compositions (see Turnock *et al.*, 1973). The b unit-cell parameter is also greatly dependent on Al content; thus care must be taken not to underestimate Fe content because of aluminum (J. J. Papike, personal communication). Differences in the b -dimensions of intergrown augite and pigeonite could not be distinguished on the X-ray precession photographs. Furthermore, b remained constant (within the uncertainty of measurement) until a crystal began to melt (Table 3)⁶, indicating constancy of Fe/Fe+Mg

in the bulk grain, further confirmed by microprobe chemical analyses (Figs. 7A and 7B).

Measurement of the unit-cell parameters of augite or pigeonite lamellae in (001) orientation with respect to the host pigeonite or augite shows that the a -dimensions of host and exsolved phase are identical within the accuracy of measurement, whereas the c -dimensions vary from one another significantly. The reverse is true for clinopyroxene lamellae in (100) orientation; the a -dimensions of host and lamellae deviate significantly and the c -dimensions are nearly identical. These observations definitely indicate that the lattices of the host and exsolved phase are constrained to fit one another along either a or c . Since both the (100) and (001) lamellae

⁶ Microprobe chemical analyses of partially melted ortho- and clinopyroxenes demonstrate that, when enough glass has formed to rim the crystals and wet the platinum foil, most of the iron is lost from the crystal and liquid.



have their b -axes oriented parallel to b of the host, the b -dimensions of host and lamellae must also be so constrained. This accounts for our inability to observe splitting of the $(0k0)$ reflections in X-ray photographs of exsolved pyroxenes. If such a constraint exists, it would clearly indicate that the use of the b unit-cell edge to determine accurate En and Fs content is suspect. Thus, the En and Fs content of the exsolved phases, plotted as circles in Figure 10, are probably not reliable and may account for some of the odd tie-line orientations, particularly Nos. 4 and 5.

The *subsolidus* homogenization data is portrayed on T - β diagrams (Fig. 9) which also show the change of Wo content of co-existing augite and pigeonite as a function of temperature. The Wo, En, and Fs content of the bulk grain are known, but the exact content of these components in the host and exsolved phases, as explained above, cannot be ascertained quantitatively.

The melting relations depicted in Figure 9 are *not* at constant bulk composition because iron leaves the pyroxene and liquid and enters the platinum. The melting relations thus shown in the solidus portion of the diagrams are for the nearly iron-free pyroxene system.

The proportion of exsolved pyroxene, relative to the total amount of the pyroxene present, is an index of the degree to which the pyroxene has been homogenized. We consistently observed that the pyroxene crystals were essentially homogenized to a single-phase pyroxene crystal just below or at the solidus temperature. Above the solidus the homogenized augite grains partially melted to yield liquid plus more Ca-rich augite (as in Figs. 9B, C, D). However, for the Ca-rich pigeonites, augite reappeared during the melting process, after the original crystal has been homogenized (see Fig. 9A). This phenomenon occurs because these bulk compositions

pass into the 3-phase region L+P+A with increasing temperature; a pyroxene phase diagram explaining this behavior is being prepared (Huebner and A. C. Turnock, unpublished data; see also Huebner and Ross, 1972).

We have made no attempt to report the degree to which a crystal has melted. Estimation of the percentage of glass is exceedingly difficult unless an ultra-thin section is made of the crystal. The nature of the melting process is being actively investigated by Huebner, Ross, and Hickling. At this time, it is only important to note evidence for first melting—tiny bubbles, and anastomosing tubules of glass. An "H" in Table 3 indicates that a crystal was intensively scrutinized for small amounts of glass, yet none was found. Melting is not observed until the liquid has coalesced into visible droplets at a temperature in excess of the actual temperature of first melting.

X-ray photographs of some augite grains which were homogenized or partially melted show the presence of two, sometimes more, augite lattices having significantly different β angles. This is noted in Table 3 (also see Fig. 9) as multiple entries of unit-cell dimensions at a single temperature of heat treatment. For example, at 1243°C, augite grain 1D (Fig. 9b) contains glass plus two crystallographically distinct augites having β angles of 106.77 and 106.08°. The presence of compositionally different augites within the same grain may be partly due to original compositional zoning where the part of the grain with higher iron content reacts at lower temperatures than does the Mg-rich portion of the grain. This is most often seen in the more highly zoned ferro-augites. Additional chemical zoning and disequilibrium conditions leading to the appearance of augites of different compositions may be caused by loss of iron from the grain to the platinum foil during the melting of pyroxene (Huebner and Ross, unpublished data).

The T -Wo sections at the temperatures of first melting, which are also the temperatures of homogenization, have been superimposed upon the pyroxene quadrilateral in Figure 10 by the addition of analytical data for En and Fs as determined by electron microprobe analysis of five homogenized clinopyroxene crystals plotted in Figure 7b. Approximate compositions for the other homogenized crystals and for the unmixed clinopyroxenes just before homogenization were determined, as previously mentioned, from the b unit-cell edge and the β

FIG. 9. Plots of temperature *vs* β angle for several host clinopyroxenes (open symbols) containing (001) exsolution lamellae (solid symbols) which were examined by X-ray precession methods between heating steps. Mole percent Wo content is estimated *semi-quantitatively* along the bottom of the figures. Compositions of some of these heated crystals are plotted in Figure 7B. Various symbols plotted represent different crystals, 1R, 3R, 3D, etc. Note that these figures are not binary phase diagrams. L is liquid.

- A. Fraction A, Ca-rich pigeonites;
- B. Fraction B, Mg-rich augites;
- C. Fraction C, augites;
- D. Fraction D, ferro-augites.

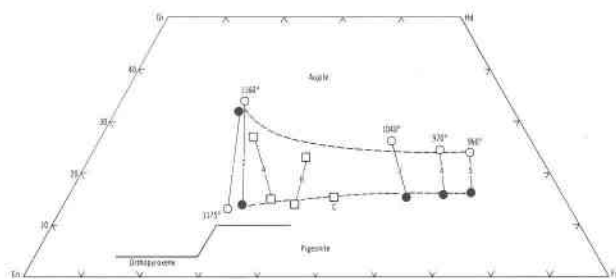


FIG. 10. Pyroxene quadrilateral showing average composition at the solidus of host augite or pigeonite crystals (open circles) and the coexisting pigeonite or augite (001) exsolution lamellae (solid circles) as determined from b - β plots and electron probe analyses (Fig. 7B). The tie lines: (1) pigeonite crystals 1R, 3R, 3D, (2) Mg-rich augite crystals 1D, 14R, 19D, 8D, (3) intermediate augite crystals 2D, 5D, (4) ferro-augite crystal 26D, and (5) ferro-augite crystal 19R, correspond to the T - W_0 sections shown in Figure 9. Temperature of homogenization ($^{\circ}\text{C}$) is given next to the open circles. The En and Fs content of the exsolved phases (solid circles) and thus the orientation of the tie-lines is poorly known due to the limitations of b in determining Mg/Mg + Fe. Also plotted, as open squares, are epitaxially overgrown augite and pigeonite in (A) grain AP-6, lunar anorthosite 15415 (Stewart *et al.*, 1972); (B) crystal 13D (Fig. 4A, B; 10); and (C) host ferropigeonite crystal P-1 (Stewart *et al.*, 1972).

angle; the determinative curves being based on our own data and that of Papike *et al.* (1971) for pyroxenes from rock 12021. In order to help delineate further the intersection of the clinopyroxene solvus and solidus, electron probe compositions of epitaxial overgrowths of augite and pigeonite from lunar basalt 12021 and lunar anorthosite 15415 are also plotted. The two-pyroxene solidus descends in temperature with increasing Fe/Mg+Fe. The solidus intersects the pyroxene solvus over the entire range of Fe/Mg compositions studied (Figs. 9, 10).

During our homogenization experiments we attempted several "reversals" to see if and at what rate unmixing could proceed. Significant unmixing under our experimental conditions occurred only in augite crystal 19D, when held for 92 hours at 1089°C after being previously heated to 1161°C , and in augite crystal 5D, when held for 238 hours at 844°C after prior heating to 1029°C . In both runs the amount of exsolved (001) pigeonite in the host increased; and the β angles of host augite and exsolved pigeonite, respectively, decreased and increased (Table 3), indicating an enrichment of calcium in the augite and depletion of calcium in the pigeonite in agreement with prediction from the experimental solvus curves. Equally long or longer

experiments on other crystals showed no apparent reversal of the homogenization process.

Discussion

Unmixing Process

Our experimental work shows that the lunar clinopyroxene host crystals redissolve the unmixed augite or pigeonite readily in the temperature range 800° to 1200°C . All experimental runs of 19 hours or greater duration appear to have come to equilibrium. The laboratory demonstration of unmixing in these same pyroxenes has proven to be much more difficult than the demonstration of homogenization. In only a few runs did we observe a significant reversal of the mixing process. The apparently large difference in rates of mixing versus unmixing suggests that the reaction mechanisms of the two processes are different.

The preservation of the compositional zoning and delicate exsolution textures in the clinopyroxenes from basalt 12021 shows that no *intergranular* recrystallization took place. The exsolution must be entirely *intragranular*, dependent only on the original composition of the grain and on pressure, temperature, cooling rates, and possibly stress. Conceivably, trace amounts of small ions, particularly hydrogen, might have some effect on the exsolution rates. We know of no experiments on silicates which would enlighten us on this problem. Our experiments on unmixing would suggest, tentatively, that the pyroxenes in lunar basalt 12021 cooled to 800°C or less over a period of at least many weeks or months.

At temperatures not far below the homogenization temperature, host pigeonites and pigeonite lamellae within augites should, if equilibrium obtains, react to form orthopyroxene ("inverted pigeonite") plus augite (Ross and Huebner, unpublished data). Such a reaction did not occur, to our knowledge, in any unshocked lunar basalt nor do we know of any observation of pigeonite lamellae in terrestrial augite reacting to form orthopyroxene. "Inverted pigeonite" textures are relatively rare, and are usually seen only in slowly cooled intrusive rocks. The nature of the process of "inversion" of pigeonite to orthopyroxene remains unknown. It appears to involve *intergranular* recrystallization and thus the probable presence of a fluid phase in the rock.

Subsolidus Phase Relations

The data plotted in Figures 9 and 10 delineate a subsolidus miscibility gap between augite and pi-

geonite compositions that extends across much of the quadrilateral. The gap is asymmetric toward pigeonite; the pigeonite solvus is steeper than the augite solvus for relatively Mg-rich compositions. This asymmetry is in accord with observed pyroxene exsolution relations in lunar rock 12021: augite exsolves 25–50 percent pigeonite, whereas pigeonite exsolves only 20–35 percent augite.

The miscibility gap does not close because these lunar pyroxenes begin to melt before the crest of the solvus is reached. At the solidus, the width of the gap narrows with increasing Fe/Fe + Mg, from about 20 percent Wo at Fe/Fe + Mg = 0.30, to about 10 percent Wo at 0.85. We have found no evidence that the solidus passes over the crest of the solvus at one atmosphere pressure; the gap persists to the most iron-rich of pyroxenes. At any Fe/Fe + Mg value, the gap for lunar basalt 12021 is narrower than the pigeonite–augite gap for any known terrestrial rock, presumably a reflection of higher f_{H_2O} and alkalis in terrestrial magmas. At higher pressure (15–16 kbar) on a synthetic join $En_{15}Fs_{85}$ -wollastonite Smith (1972) has found a symmetrical solvus with a crest at 915–950°C. The differences in shape and position are attributable to experimental error and differences in pressure and composition.

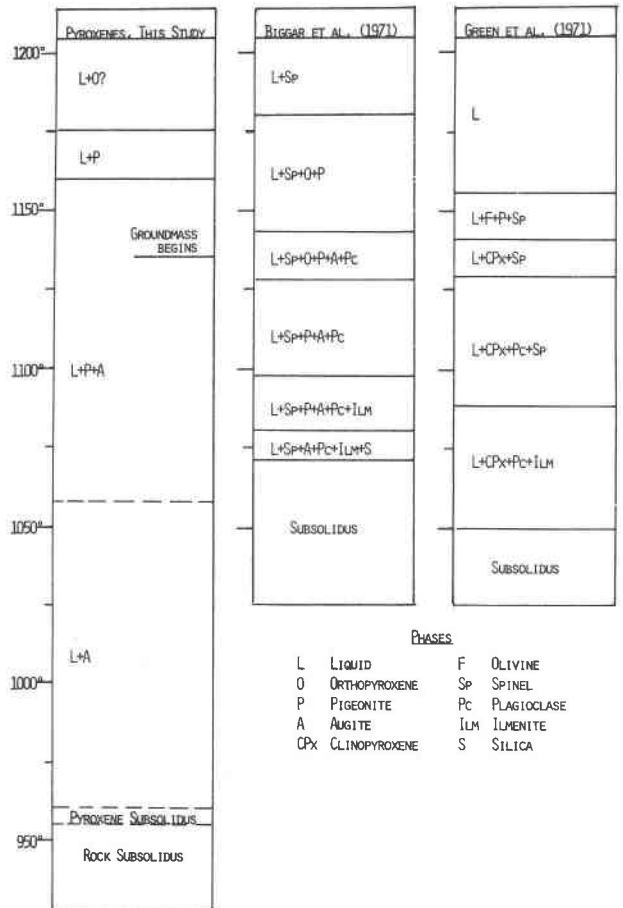
The melting temperatures observed in this study, 960–1175°C, are considerably lower than the temperatures found in phase-relation studies of synthetic pyroxene systems. Roedder (1965) found that the lowest liquidus temperature for synthetic (En–Fs–Hd–Di) quadrilateral compositions was 1160°C on the Hd–Fs join, implying solidus temperatures no lower than 1160°. Yoder *et al* (1964) melted natural pyroxenes and pyroxene mixtures; they found solidus temperatures between those found by Roedder and those presented in this study. These differences may be due to the presence of minor additional components (Huebner and Turnock, unpublished data; Huebner, Ross, and Hickling, unpublished data; see also Huebner *et al*, 1972).

Geothermometry

Our work places constraints on the crystallization temperature range of lunar rock 12021 and similar rocks. Exsolution features develop from initially homogeneous pyroxenes; therefore, a pyroxene must have crystallized at a temperature equal to or exceeding its homogenization temperature. However, a pyroxene will crystallize from a natural magma

at a temperature that is lower than the melting temperature of pyroxene alone. The homogenization and melting temperatures, which seem to be indistinguishable, suggest cotectic crystallization of the two pyroxenes in the original rock and provide an excellent estimate of the possible range of pyroxene crystallization temperature: 1175° ± 15° to 960° ± 15°C. Since these pyroxenes crystallized throughout much of the crystallization process of lunar rock 12021, these temperatures also indicates the approximate range of crystallization for the bulk rock. Consideration of the textural relationships indicates that some of the spinel may have crystallized at temperatures higher than 1175°C; most pyroxferroite and all silica crystallized below 960°C. Our estimate of the temperature of initial pyroxene crystallization (Table 4) is in general agreement with the temperatures obtained from whole-rock crystallization and melting studies; however, we are

TABLE 4. Crystallization Temperatures: Lunar Rock 12021 at 1 Atm.



better able to define the lower temperature crystallization range (1100°–960°C), and we have shown that pyroxene crystallization continued to at least 960°C.

Acknowledgments

We wish to thank the several people who contributed time or equipment to this study. Miss Mary Woodruff, U.S. Geological Survey, prepared reams of microprobe data for computer reduction with the program ABFAN, written by Dr. Larry Finger, of the Geophysical Laboratory, Carnegie Institution of Washington; she also typed versions of the manuscript. Dr. Finger also made available to Huebner the Geophysical Laboratory's automated microprobe for one operating shift, resulting in 68 fully reduced 8-element analyses. Professor A. E. Bence, State University of New York at Stony Brook, analyzed by electron microprobe most of the heat-treated pyroxene grains plotted in Figure 10. Mr. Nelson Hickling, U.S. Geological Survey, assisted Huebner in making the remaining 228 spot analyses plotted in Figures 3 and 10. We have benefitted from interesting discussions with numerous individuals and would like to mention in particular Professors Donald H. Lindsley and James J. Papike, State University of New York at Stony Brook, and Dr. F. R. Boyd, Geophysical Laboratory, Carnegie Institution of Washington. This investigation was in part supported by NASA.

References

- BENCE, A. E., AND J. J. PAPIKE (1972) Pyroxenes as recorders of lunar basalt petrogenesis: Chemical trends due to crystal-liquid interaction. *Proc. Third Lunar Sci. Conf.* **1**, 431–469, M.I.T. Press.
- , ———, AND C. T. PREWITT (1970) Apollo 12 clinopyroxenes: Chemical trends. *Earth Planet. Sci. Lett.* **8**, 393–399.
- , ———, AND D. H. LINDSLEY (1971) Crystallization histories of clinopyroxenes in two porphyritic rocks from Oceanus Procellarum. *Proc. Second Lunar Sci. Conf.* **1**, 559–574, M.I.T. Press.
- BIGGAR, G. M., M. J. O'HARA, A. PECKETT, AND D. J. HUMPHRIES (1971) Lunar lava and the achondrites. Petrogenesis of protohypersthene basalts in the maria lava lakes. *Proc. Second Lunar Sci. Conf.* **1**, 617–643, M.I.T. Press.
- BOYD, F. R., AND D. SMITH (1971) Compositional zoning in pyroxenes from lunar rock 12021. *Oceanus Procellarum. J. Petrology*, **12**, 439–464.
- CUTTITTA, F., H. J. ROSE, JR., C. S. ANNELL, M. K. CARRON, R. P. CHRISTIAN, E. J. DWORNIK, L. P. GREENLAND, A. W. HELZ, AND D. T. LIGON, JR. (1971) Elemental composition of some Apollo 12 lunar rocks and soils. *Proc. Second Lunar Sci. Conf.* **2**, 1217–1229, M.I.T. Press.
- DARKEN, L. S., AND R. W. GURRY (1945) The system iron-oxygen. I. The wustite field and related equilibria. *J. Amer. Chem. Soc.* **67**, 1398–1412.
- DENCE, M. R., J. A. V. DOUGLAS, A. G. PLANT, AND R. J. TRAILL (1971) Mineralogy and petrology of some Apollo 12 samples. *Proc. Second Lunar Sci. Conf.* **1**, 285–299, M.I.T. Press.
- DOWTY, E., M. ROSS, AND F. CUTTITTA (1972) Fe²⁺-Mg site distribution in Apollo 12 clinopyroxenes: Evidence for bias in Mossbauer spectra, and relation of ordering to exsolution. *Proc. Third Lunar Sci. Conf.*, **1**, 481–492, M.I.T. Press.
- ENGEL, A. E. J., C. G. ENGEL, A. L. SUTTON, AND A. T. MYERS (1971) Composition of five Apollo 11 and Apollo 12 rocks and one Apollo 11 soil and some petrogenic considerations. *Proc. Second Lunar Sci. Conf.* **1**, 439–448, M.I.T. Press.
- FERNANDEZ-MORAN, H., M. OHTSUKI, AND H. HIBINO (1971) Correlated electron microscopy and diffraction of lunar clinopyroxenes from Apollo 12 samples. *Proc. Second Lunar Sci. Conf.* **1**, 109–116, M.I.T. Press.
- GREEN, D. H., A. E. RINGWOOD, N. G. WARE, W. O. HIBBERSON, A. MAJOR, AND E. KISS (1971) Experimental petrology and petrogenesis of Apollo 12 basalts. *Proc. Second Lunar Sci. Conf.* **1**, 601–615, M.I.T. Press.
- HOLLISTER, L. S., W. E. TRZCIENSKI, JR., R. B. HARGRAVES, AND C. G. KULICK (1971) Petrogenetic significance of pyroxenes in two Apollo 12 samples. *Proc. Second Lunar Sci. Conf.* **1**, 529–557, M.I.T. Press.
- HUEBNER, J. S., AND M. SATO (1970) The oxygen fugacity-temperature relationships of manganese oxide and nickel oxide buffers. *Amer. Mineral.* **55**, 934–952.
- , AND M. ROSS (1972) Phase relations of lunar and terrestrial pyroxenes at one atm. In, C. Watkins, Ed., *Lunar Science III, Lunar Science Institute Contrib.* **88**, 410–412.
- , ———, AND A. C. TURNOCK (1972) Phase diagrams for pyroxene compositions (abstr.). *Geol. Soc. Amer. Abstr. Programs*, **4**, 547.
- JAMES, O. B., AND T. L. WRIGHT (1972) Apollo 11 and 12 mare basalts and gabbros: Classification, compositional variations and possible petrogenetic relations. *Bull. Geol. Soc. Amer.* **83**, 2357–2382.
- KLEIN, C., JR., J. C. DRAKE, AND C. FRONDEL (1971) Mineralogical, petrological, and chemical features of four Apollo 12 lunar microgabbros. *Proc. Second Lunar Sci. Conf.* **1**, 265–284, M.I.T. Press.
- KUSHIRO, I., AND H. HARAMURA (1971) Major element variation and possible source materials of Apollo 12 crystalline rocks. *Science*, **171**, 1235–1237.
- NAFZIGER, R. H., G. C. ULMER, AND E. WOERMAN (1971) Gaseous buffering for the control of oxygen fugacity at one atmosphere. In, G. C. Ulmer, Ed., *Research techniques for high pressure and high temperature*, New York, Springer Verlag, pp. 9–41.
- PAPIKE, J. J., A. E. BENCE, G. E. BROWN, C. T. PREWITT, AND C. H. WU (1971) Apollo 12 clinopyroxenes. Exsolution and epitaxy. *Earth Planet. Sci. Lett.* **10**, 307–315.
- ROEDDER, E. (1965) A laboratory reconnaissance of the liquidus surface in the pyroxene system En–Di–Hd–Fs (MgSiO₃–CaMgSi₂O₆–CaFeSi₂O₆–FeSiO₃). *Amer. Mineral.* **50**, 696–703.
- ROSS, M., J. J. PAPIKE, AND K. W. SHAW (1969) Exsolution textures in amphiboles as indicators of subsolidus thermal histories. *Mineral Soc. Amer. Spec. Pap.* **2**, 275–299.

- , J. S. HUEBNER, AND E. DOWTY (1971a) Melting and sub-solidus phase relations of augite and pigeonite from lunar rock 12021. *Apollo 12 Lunar Sci. Conf.* (unpublished proceedings).
- , ———, AND ——— (1971b) Delineation of the one atmosphere augite-pigeonite solvus and orthopyroxene-pigeonite reaction curve, and pigeonite melting relations (abstr.). *Geol. Soc. Amer. Abstr. Programs*, **3**, 690.
- SATO, M. (1970) An electrochemical method of oxygen fugacity control of furnace atmosphere for mineral synthesis. *Amer. Mineral.* **55**, 1424–1431.
- (1971) Electrochemical measurements and control of oxygen fugacity and other gaseous fugacities with solid electrolyte sensors. In, G. C. Ulmer, Ed., *Research techniques for high pressure and high temperature*, New York, Springer Verlag, pp. 43–99.
- SMITH, D. (1972) Stability of iron-rich pyroxene in the system $\text{CaSiO}_3\text{--FeSiO}_3\text{--MgSiO}_3$. *Amer. Mineral.* **57**, 1413–1428.
- STEWART, D. B., M. ROSS, B. A. MORGAN, D. E. APPLEMAN, J. S. HUEBNER, AND R. F. COMMEAU (1972) Mineralogy and petrology of lunar anorthosite 15415. In, C. Watkins, Ed., *Lunar Science III, Lunar Science Inst. Contrib.* **88**, 726–728.
- TURNOCK, A. C., D. H. LINDSLEY, AND J. E. GROVER (1973) Synthesis and unit cell parameters of Ca-Mg-Fe pyroxenes. *Amer. Mineral.* **58**, 50–59.
- WALTER, L. S., B. M. FRENCH, K. F. J. HEINRICH, P. D. LOWMAN, JR., A. S. DOAN, AND I. ADLER (1971) Mineralogical studies of Apollo 12 samples. *Proc. Second Lunar Sci. Conf.* **1**, 343–358, M.I.T. Press.
- WEILL, D. F., R. A. GRIEVE, I. S. MCCALLUM, AND Y. BOTTINGA (1971) Mineralogy-petrology of lunar samples. Microprobe studies of samples 12021 and 12022; viscosity of melts of selected lunar compositions. *Proc. Second Lunar Sci. Conf.* **1**, 413–430, M.I.T. Press.
- YODER, H. S., JR., C. E. TILLEY, AND J. F. SCHAIRER (1964) Isothermal sections of pyroxene quadrilateral. *Carnegie Inst. Washington Year Book*, **63**, 121–129.

*Manuscript received, November 15, 1972;
accepted for publication, February 13, 1973.*